PROCEEDINGS OF SPIE

SPIEDigitalLibrary.org/conference-proceedings-of-spie

Intensity uniformity optimization in spatial-light-modulator-based multifocal microscope

Amin, M. Junaid, Petry, Sabine, Yang, Haw, Shaevitz, Joshua

M. Junaid Amin, Sabine Petry, Haw Yang, Joshua W. Shaevitz, "Intensity uniformity optimization in spatial-light-modulator-based multifocal microscope," Proc. SPIE 11649, Three-Dimensional and Multidimensional Microscopy: Image Acquisition and Processing XXVIII, 116490P (5 March 2021); doi: 10.1117/12.2578859



Event: SPIE BiOS, 2021, Online Only

Intensity uniformity optimization in spatial-light-modulator-based multifocal microscope

M. Junaid Amin^{a,b,c,d}, Sabine Petry^a, Haw Yang^b and Joshua W. Shaevitz*,c,d

aDepartment of Molecular Biology, Princeton University, Princeton, New Jersey 08544, USA;

bDepartment of Chemistry, Princeton University, Princeton, New Jersey 08544, USA;

cLewis-Sigler Institute for Integrative Genomics, Princeton University, Princeton, New Jersey 08544, USA;

dDepartment of Physics, Princeton University, Princeton, New Jersey 08544, USA

*shaevitz@princeton.edu

ABSTRACT

Multifocal microscopes (MFMs) are becoming increasingly popular in fluorescence microscopy due to their high speed three-dimensional (3D) imaging capabilities. Conventional MFMs use a fixed fabricated grating as the multifocal grating but these are limited to a restricted wavelength range and a fixed object-plane separation. Spatial light modulators (SLMs) represent an alternative to fabricated gratings due to their real-time programmability, providing complete control over emission wavelength range and object plane separations. However, algorithms commonly used to obtain multifocal grating patterns which provide uniform intensity across the subimages are not directly applicable to SLM-based MFMs due to inherent pixel-to-pixel crosstalk effects present in the SLM chip. We recently developed an *in-situ* iterative algorithm which generates grating patterns that provide near-uniform illumination of the subimages in SLM-based MFMs. This algorithm is universal across wavelengths, object-plane separations, and SLM manufacturers. As part of our efforts to develop an SLM-based MFM that can respond rapidly to changing experimental parameters, we implement a gradient descent-based optimization method. We evaluate its performance in comparison with a grid search based routine. Experimental results obtained on a custom-made SLM-based MFM indicate that the grid-search optimized grating patterns provide superior subimage intensity uniformity versus the gradient-descent method. These experiments also provide an insight into the energy landscape involved in these optimizations. This study increases the utility of SLM-based MFMs in high-speed imaging.

Keywords: Multifocal microscopy, multiplane microscopy, 3D imaging, spatial light modulator, optical feedback control, darkfield microscopy

1. INTRODUCTION

Three-dimensional (3D) fluorescence imaging technologies have rapidly evolved over the past decades^[1, 2]. Multifocal microscopy is a promising technique that enables imaging of multiple axially separated object planes simultaneously with a single camera^[3-5]. This is commonly achieved by directing the sample scattered or fluorescence emission through a custom designed grating, known as a multifocal grating. The multifocal grating is uniquely patterned such that it generates multiple diffraction orders, with each order having a unique degree of defocus associated with it^[6, 7]. These orders are imaged side by side onto a camera sensor resulting in a 3D image where different regions of the sensor, which are denoted as subimages in this paper, correspond to different object planes. In such systems, up to a hundred or more 3D sample volumes per second can be recorded since the only hardware limiting factor to the 3D volume imaging speed is the frame rate of the camera.

Although fabricated gratings have been widely used in the literature as multifocal gratings^[3, 4], SLMs are becoming increasing popular due to their versatility and real-time programmability^[5, 8]. Parameters such as object plane separations and emission wavelength can readily be changed using SLMs without physically changing any grating optics. However, obtaining SLM patterns which achieve uniform intensity in the multifocal subimages has been challenging due to SLM pixel-to-pixel crosstalk effects.

Recently, an *in-situ* iterative algorithm was developed to overcome this issue to provide near-uniform subimage intensities. The method is based on a feedback process which uses a metric obtained from real-time acquired camera images in a multifocal microscope to optimize the programmable SLM pattern to provide uniform intensities across the subimages^[5]. In such a scenario, the parameter space being considered is composed of the gray-level values of all the pixels making up the SLM pattern. Since the SLM pattern is a grating pattern made up of repeating unit cells,

Three-Dimensional and Multidimensional Microscopy: Image Acquisition and Processing XXVIII, edited by Thomas G. Brown, Tony Wilson, Laura Waller, Proc. of SPIE Vol. 11649, 116490P © 2021 SPIE · CCC code: 1605-7422/21/\$21 · doi: 10.1117/12.2578859

we only optimize the unit cells which has dimensions $P_u \times P_u$ pixels². The desired global optimum is thus a location in this parameter space which achieves the highest subimage intensity uniformity. In the initial work^[5], a grid search routine was implemented as part of the optimization portion of the *in-situ* iterative algorithm. Although near-uniform intensities are achieved and reported, the computational cost of grid search methods is high since it spans a large portion of the parameter space in search of the global optima. In this work, we implement a gradient descent-based approach as part of the *in-situ* iterative algorithm optimization in an effort to find the global optimum more efficiently. We compare the experimental performance of the gradient descent-based routine versus the grid search algorithm in the framework of the *in-situ* iterative algorithm, and show that the grid search allows high subimage intensity uniformities.

The rest of the paper is organized as follows. A brief description of the experimental setup is first provided. This is followed by description of the grid-search and the gradient descent algorithms as implemented in the pattern optimization framework. The results of the two methods are subsequently presented and discussed, followed by a conclusion summarizing the work.

2. MULTIFOCAL MICROSCOPE OPTICAL SETUP

The multifocal microscope optical diagram is shown in Figure 1. Briefly, an excitation laser passes through Lens 1, dichroic and a microscope objective onto the sample. Lens 1 focuses the beam onto the back focal plane of the objective to realize uniform illumination of the sample. Emission/scattering from the sample collected by the objective is reflected by a dichroic towards Lens 2 which forms an image at the Rectangular Aperture that controls the imaging field of view. Lens 3 forms the Fourier plane at the reflective SLM which displays the multifocal grating pattern. $N \times N$ array of diffraction orders emanate from the SLM (N = 3 shown in Fig. 1) and imaged onto the camera sensor through an emission filter. A linear polarizer (not shown) is positioned in the emission path to ensure linear polarization of the emission necessary for the phase-only SLM operation. The microscope also functions in darkfield/brightfield modalities by including additional illumination optics above the sample (not shown in Fig. 1). A detailed description of the setup is provided in the previous work^[5].

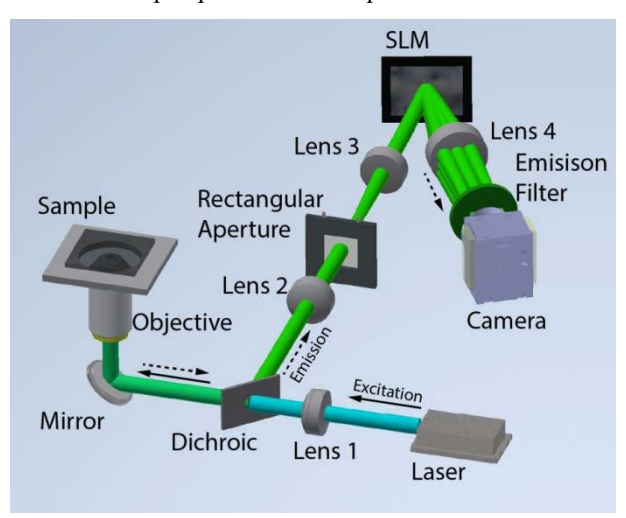


Figure 1. Optical diagram of the multifocal microscope.

3. OPTIMIZATION ALGORITHMS

The multifocal grating pattern displayed on the SLM is composed of repeating unit cells having dimensions of $P_u \times P_u$ pixels². The phase values of the SLM pixels are governed by the gray-level values of the images displayed on the SLM. The *in-situ* iterative algorithm finds an optimal set of gray-level values for the repeating $P_u \times P_u$ pixels² region of the SLM such that near uniform intensities are observed in the image plane. This is done iteratively using information from the camera images. The metric used to evaluate the uniformity of multifocal subimages is given by^[5]:

$$M = \frac{\min(\lbrace I_{m,i} \rbrace) - I_b}{\max(\lbrace I_{m,i} \rbrace) - I_b},\tag{1}$$

where $\{I_{m,i}\}$ is the measured intensity in subimage i ($i = 1 \dots N \times N$) and I_b is a measured background intensity. M ranges from 0 to 1, with M=1 corresponding to completely uniform subimage intensities. M can be computed using multifocal microscope imaging in fluorescence as well as scattering imaging operation modes. The two optimization routines discussed in this manuscript which maximize M are the grid search and the gradient descent methods. Figure 2 shows a step-by-step sequence for both techniques. Both methods assume a randomized initial starting pattern.

3.1 Grid Search Algorithm

The grid search algorithm^[9] starts by randomly choosing a pixel on the unit cell. The gray-level value of this pixel only is changed sequentially to cover the 0-255 gray-level range typical for SLMs. The step size of each gray-level change, denoted as η , is empirically chosen. For each change, M is measured using the corresponding image. If any measured M is greater than the previous best M, the gray-level value for that pixel is updated. Once all gray-levels are covered for the first pixel, another randomly chosen pixel is selected and the process is repeated. This is done for all pixels within the $P_u \times P_u$ unit cell. The cycle is repeated a few times until there is no change in M over a complete scan of the unit cell.

Note that, for a single scan of the entire unit cell, one can compute the total number of images needed to be acquired. Assuming an 8-bit SLM display, the total addressable gray-level values are $256/\eta$. The total images acquired in a single scan are $P_u \times P_u \times 256/\eta$. If the grid search runs for N_{gs} iterations, the total images acquired will be $P_u \times P_u \times 256/\eta \times N_{gs}$. This quantity of the number of images is useful to estimate the computational and time cost of the algorithm. This will be discussed further in the experimental results section.

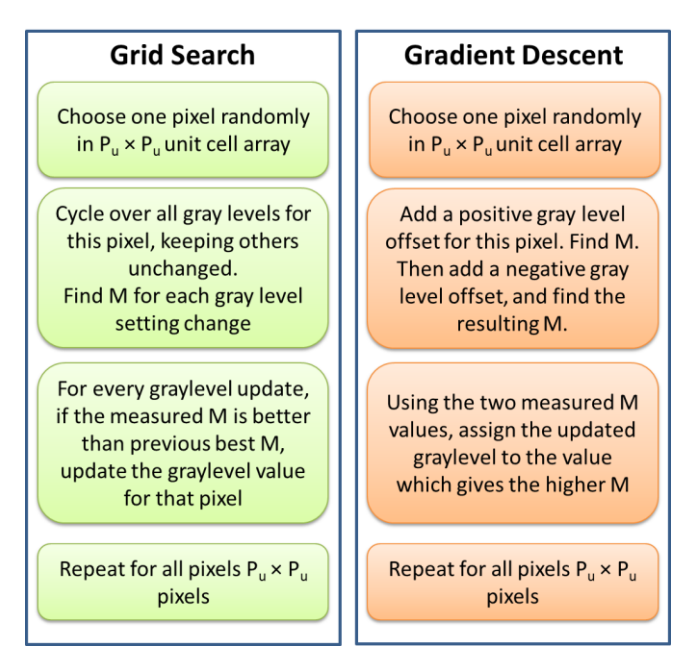


Figure 2. Step-by-step description of grid search and gradient descent routines implemented as part of the *in-situ* iterative algorithm.

3.2 Gradient Descent Algorithm

The gradient descent algorithm^[10] begins by selecting a random pixel in the unit cell. For this pixel, a positive gray-level offset ε is applied and the resulting M is measured. Next, a negative gray-level offset $-\varepsilon$ is applied for this same pixel, keeping the rest of the pixels unchanged, and M is measured. The new gray-level value of this pixel is set to the value which gives the higher M of the two measured. Next, another pixel is randomly chosen and the process is repeated until all pixels in the unit cell are covered. This cycle is repeated for an empirically chosen N_{gd} times.

The total number of images in a single unit-cell scan for gradient descent is $P_u \times P_u \times 2$. Assuming N_{gd} full cycles, the total images acquired are $P_u \times P_u \times 2 \times N_{gd}$.

4. EXPERIMENTAL RESULTS

Both grid search and gradient descent methods are implemented as part of the *in-situ* iterative algorithm based in LABVIEW and executed on a home-built multifocal microscope in brightfield configuration, see ref. [16] for a detailed description of the optical components used. The sample is an empty coverslip with brightfield illuminating optics from the top. The SLM used is Holoeye Pluto-VIS-056 having a pixel size of 8 μm, the emission filter used is centered at 685 nm with a bandwidth of 15 nm, and the camera used is Hamamatsu's Orca Flash 4 V3. For M measurements, $I_{m,i}$ is measured as the mean intensity across a 30 \times 30 pixels² region on the camera within each subimage. I_b is measured by switching off the brightfield lamp and measuring the mean intensity of a camera region of the same size. The experimental parameters used are $P_u = 4$ and N = 3. For grid search, $\eta = 3.2$ which corresponds to 256 gray-levels divided coarsely into 80 segments. We empirically found that dividing the 8-bit gray-level range into finer steps did not yield improved performance. Ngd was experimentally observed to be between fall between 6 and 10 (average of 8). For gradient descent, $\varepsilon = 5$ is empirically chosen; a smaller ε results in issues of running into a local minimum while a large ε value could result in overshooting the ideal maximum in the parameter space. N_{gd} is set to 150 to allow sufficient iterations for gradient descent convergence. The mean total number of images acquired during a grid search execution is $P_u \times P_u \times 256/\eta \times N_{gs} = 4 \times 4 \times 256/3.2 \times 8 = 10,240$ images. For gradient descent, this number is computed as $P_u \times P_u \times 2 \times N_{gd} = 4 \times 4 \times 2 \times 150 = 4,800$ images. The camera exposure time is set to 20 ms and the time duration between each gray-level change (which includes the camera exposure and image processing for M computation) is ~ 120 ms. Therefore, on average it takes ~ 20 minutes to run the grid search algorithm and ~10 minutes to run a gradient descent optimization using the parameters used.

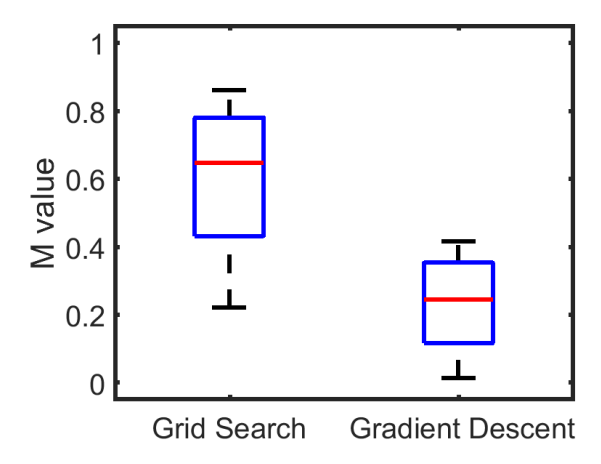


Figure 3. M value comparison of grid search and gradient descent methods, 18 iterations in each.

A boxplot of the *M* values resulting from the grid search (6 iterations) and the gradient descent (18 iterations) methods is shown in Figure 3. According to Figure 3, the grid search method provides higher subimage uniformity versus the gradient descent method across multiple iterations. This indicates that the grid search method is more suited to provide higher uniformity in multifocal imaging given the experimental parameters used. Example data points from the Figure 3 plot are chosen for both grid search and gradient descent methods, and the corresponding optimized pattern-resulting brightfield images are obtained optimized pattern are shown in Figure 4. Figure 4(a)

shows a brightfield image, having M = 0.78, obtained using a grid search optimized pattern, whereas Figure 4(b) shows a brightfield image, having M = 0.35, obtained using a gradient descent optimized SLM pattern.

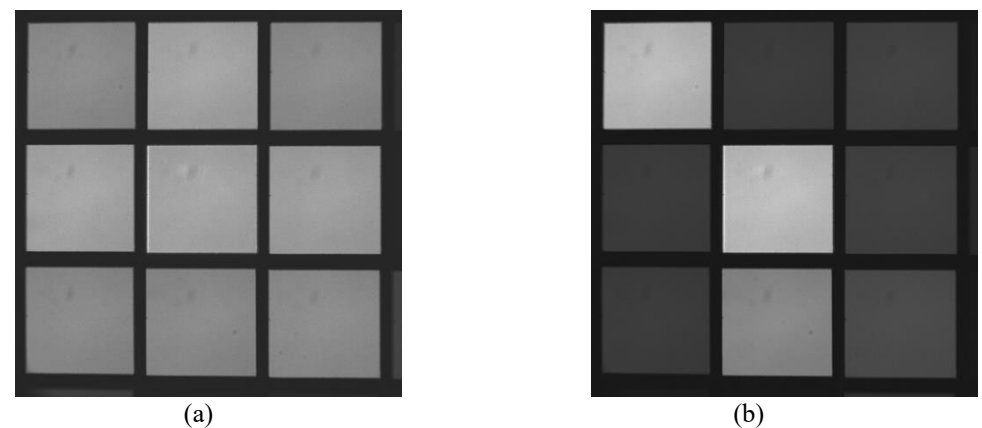


Figure 4. Example brightfield multifocal images ($\Delta z = 0$) using optimized SLM patterns using (a) grid search with M = 0.78, and (b) gradient descent M = 0.35.

5. DISCUSSION

Although the gradient descent runs two times faster than the grid search method in our implementation, the grid search method provides better uniformity performance compared to the gradient descent method, as implemented in the *in-situ* iterative algorithm framework. A closer analysis of how *M* evolves during the optimization process for both grid search and gradient descent methods is presented in Figure 5 which shows the *M* values measured for each acquired image in real-time (blue data points) versus the best *M* values up to that point (red data points). Figure 5(a) shows how *M* values progress versus acquired image number for the grid search method. Note that because the grid search spans a large parameter space, a large spread in the *M* values for each acquired image is observed. On the other hand, the Figure 5(b) *M* values for the gradient descent execution show a narrow spread of the *M* values as the gray-level pattern is updated in each step. This narrow *M* variation of real-time acquired images (blue data points) expected since gradient descent directly moves towards the optimum without sampling other regions in the parameter space. The poor performance of the gradient descent as shown in Figure 3 could be due to the presence of multiple local optima. On the other hand, the grid search does not seem to suffer from this problem and is better suited to find the global optimum for this type of problem, compared to the current gradient descent implementation in the this framework. This is because of the different paths (and steps) that the grid search and gradient descent take in the energy landscape.

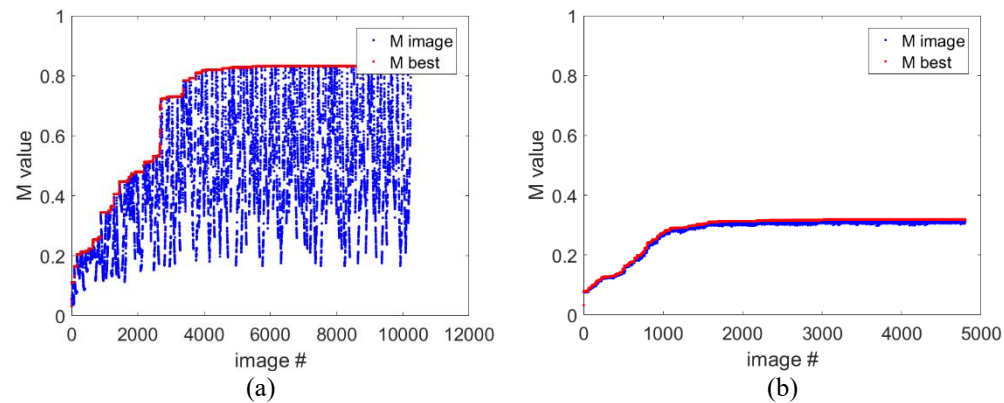


Figure 5. Plots showing the progression of M versus each image acquired in (a) grid search, and (b) gradient descent

In addition to indicating the complexity of the optimization energy landscape, Figure 5 also indicates that the convergence of gradient descent is nearly 4 times faster (~1000 steps vs ~4000 steps) than that of grid search. It is straightforward to apply a convergence criterion for the gradient descent so that it stops when there is minimal update to the metric. Even though the gradient descent does not converge to an optimal subimage uniformity location, at least for the current metric used, it is several folds faster and can be a useful prototyping method for multifocal microscopy when trying new fluorescent dyes, emission wavelengths as well as SLM calibration settings and object plane separations. Once experimental settings are finalized, the grid search algorithm can then be used to find optimal SLM patterns for more quantitative experiments and data acquisition.

In literature, there are variations of the gradient descent^[11] as well as other optimization routines, which help deal with the complex optimization energy landscape in the SLM pattern optimization process. Implementing more involved optimization routines will be a subject of future work to further improve the *in-situ* iterative method for intensity uniformity in multifocal microscopes. This also presents an interesting academic problem for researchers pushing towards improving microscopy using computational expertise.

6. CONCLUSION

We present an analysis of grid search and gradient descent algorithms as optimization methods as part of the *in-situ* iterative method to acquire SLM patterns providing near-uniform multifocal subimage intensities. Experimental results suggest that the grid search is more suited for obtaining optimized SLM patterns, whereas gradient descent converges much faster but could converge to local optima within the parameter space. Future work will look at other optimization algorithms in an effort to minimize the computational cost as well as maximize illumination uniformity in multifocal microscopy.

REFERENCES

- [1] Denk, W., J.H. Strickler, and W.W. Webb,"Two-photon laser scanning fluorescence microscopy,"Science. **248**(4951), p. 73-6, (1990).
- [2] Huisken, J., et al., "Optical Sectioning Deep Inside Live Embryos by Selective Plane Illumination Microscopy," Science. **305**(5686), p. 1007, (2004).
- [3] Dalgarno, P.A., et al.,"Multiplane imaging and three dimensional nanoscale particle tracking in biological microscopy,"Optics Express. **18**(2), p. 877-884, (2010).
- [4] Abrahamsson, S., et al.,"Fast multicolor 3D imaging using aberration-corrected multifocus microscopy,"Nature Methods. **10**(1), p. 60-63, (2013).
- [5] Amin, M.J., et al., "Uniform intensity in multifocal microscopy using a spatial light modulator," PLOS ONE. **15**(3), p. e0230217, (2020).
- [6] Lee, W.-H., "Binary computer-generated holograms," Applied Optics. 18(21), p. 3661-3669, (1979).
- [7] Blanchard, P.M. and A.H. Greenaway, "Simultaneous multiplane imaging with a distorted diffraction grating," Applied Optics. **38**(32), p. 6692-6699, (1999).
- [8] Ma, Q., et al., "Three-dimensional fluorescent microscopy via simultaneous illumination and detection at multiple planes," Scientific Reports. 6(1), p. 31445, (2016).
- [9] Yakowitz, S.J. and L. Fisher,"On sequential search for the maximum of an unknown function, "Journal of Mathematical Analysis and Applications. **41**(1), p. 234-259, (1973).
- [10] Curry, H.B.,"THE METHOD OF STEEPEST DESCENT FOR NON-LINEAR MINIMIZATION PROBLEMS,"Quarterly of Applied Mathematics. **2**(3), p. 258-261, (1944).
- [11] Noel, M.M.,"A new gradient based particle swarm optimization algorithm for accurate computation of global minimum,"Applied Soft Computing. **12**(1), p. 353-359, (2012).